Cell Reports
Physical Science

CellPress
OPEN ACCESS

Article

Tuning pH-dependent cytotoxicity in cancer cells by peripheral fluorine substitution on pseudopeptidic cages

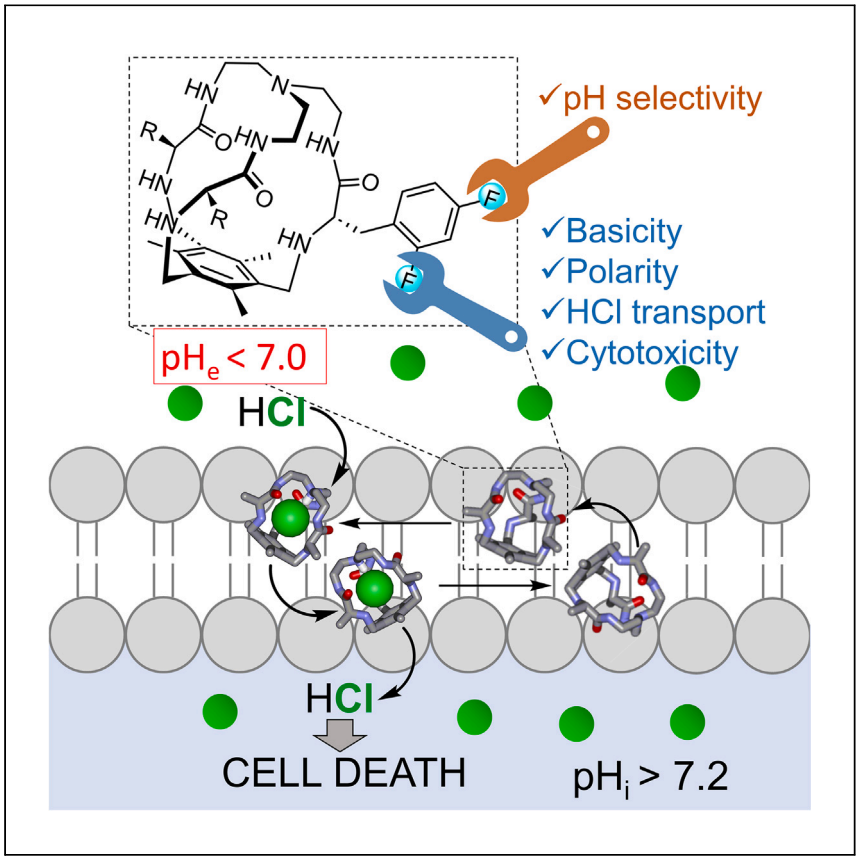

Tapia et al. report that specific fluorine substitutions on the side chains of HCl-binding pseudopeptidic cages modulate their physicochemical properties and behavior at the aqueous-lipid interphase. Unraveling the transport mechanism leads to pH-dependent ionophores that kill cancer cells at the acidic pH around solid tumors, being essentially non-toxic at the pH of healthy tissues.

Lucía Tapia, Yolanda Pérez, Israel Carreira-Barral, ..., Jordi Solà, Roberto Quesada, Ignacio Alfonso

ignacio.alfonso@iqac.csic.es

Highlights

Fluorine-substituted pseudopeptidic cages bind and transport HCl through lipid membranes

Their physicochemical properties define their behavior at the aqueous-lipid interphase

Cages with specific F substitutions show pH-dependent cytotoxicity in cancer cells

Optimized cages are toxic at the pH around tumors but non-toxic at physiological pH

Tapia et al., Cell Reports Physical Science 5, 102152
September 18, 2024
https://doi.org/10.1016/j.xcrp.2024.102152

Cell Reports
Physical Science

CellPress
OPEN ACCESS

Article

Tuning pH-dependent cytotoxicity in cancer cells by peripheral fluorine substitution on pseudopeptidic cages

Lucía Tapia,[1] Yolanda Pérez,[2] Israel Carreira-Barral,[3] Jordi Bujons,[1] Michael Bolte,[4] Carmen Bedia,[5] Jordi Solà,[1] Roberto Quesada,[3] and Ignacio Alfonso[1,6,*]

SUMMARY

The acidic microenvironment of solid tumors is a potential source of selectivity in the anti-cancer activity of ionophores, which requires delicate control of their biophysical properties. In this context, we have systematically studied fluorine substitutions in the aromatic side chains of HCl-binding pseudopeptidic cages. Interconnected factors like chloride binding, protonation, lipophilicity, and conformation and diffusiveness of the cages can impact their ability to transport HCl through the aqueous-lipid interphase, as demonstrated by robust experimental (X-ray, nuclear magnetic resonance [NMR], fluorescence) and theoretical results. The fine-tuning of these properties allows the modulation of their pH-dependent cytotoxicity against cancer cells, from essentially non-cytotoxic at pH 7.5 (like the extracellular surroundings of healthy tissues) to highly toxic in slightly acidic microenvironments (like those around solid tumors). Thus, a distal fluorine substitution produces a big impact on the physicochemical and biological properties of the cages, improving their selectivity as potential therapeutic ionophores.

INTRODUCTION

Cancer is among the deadliest human diseases,[1,2] making the discovery of new approaches for therapies a hot topic in scientific research.[3–6] Although the use of synthetic molecules to kill cancer cells is still one of the most widely used therapies (so-called chemotherapy),[7–9] it still has to overcome important drawbacks. First of all, most of the used anti-cancer molecules show low specificity,[10–12] thus producing serious and sometimes unacceptable side effects. Besides, the high mutation rate of cancer cells allows them to rapidly evolve and develop chemoresistance[13–16] by circumventing the action of the administered drug on the biochemical target. Regarding this last issue, the use of synthetic ionophores as anti-cancer prospective drugs[17–20] has appeared as a promising option[20–26] since their mechanism of action hampers the easy development of resistance by cancer cells.[17,19,27,28] However, very often, these ionophores show little selectivity, thus being also toxic to healthy cells and therefore unsuitable for further development as real-life drugs.[19,23] Paradoxically, the appealing mechanism of action of ionophores targeting cell membranes complicates the necessary implementation of selectivity.

On the other hand, pH dysregulation is a hallmark of cancer,[29,30] with abnormally reversed pH gradients between extracellular and intracellular values (Figure 1A). Thus, cancer cells are characterized by intracellular alkalinization and extracellular acidification.[31] As a consequence, solid tumors are surrounded by a slightly acidic

[1]Department of Biological Chemistry, Institute for Advanced Chemistry of Catalonia, IQAC-CSIC, 08034 Barcelona, Spain

[2]NMR Facility, Institute for Advanced Chemistry of Catalonia, IQAC-CSIC, 08034 Barcelona, Spain

[3]Departamento de Química, Facultad de Ciencias, Universidad de Burgos, 09001 Burgos, Spain

[4]Institut für Anorganische Chemie, J.-W.-Goethe-Universität, 60438 Frankfurt/Main, Germany

[5]Institute of Environment Assessment and Water Research, IDAEA-CSIC, 08034 Barcelona, Spain

[6]Lead contact

*Correspondence: ignacio.alfonso@iqac.csic.es

https://doi.org/10.1016/j.xcrp.2024.102152

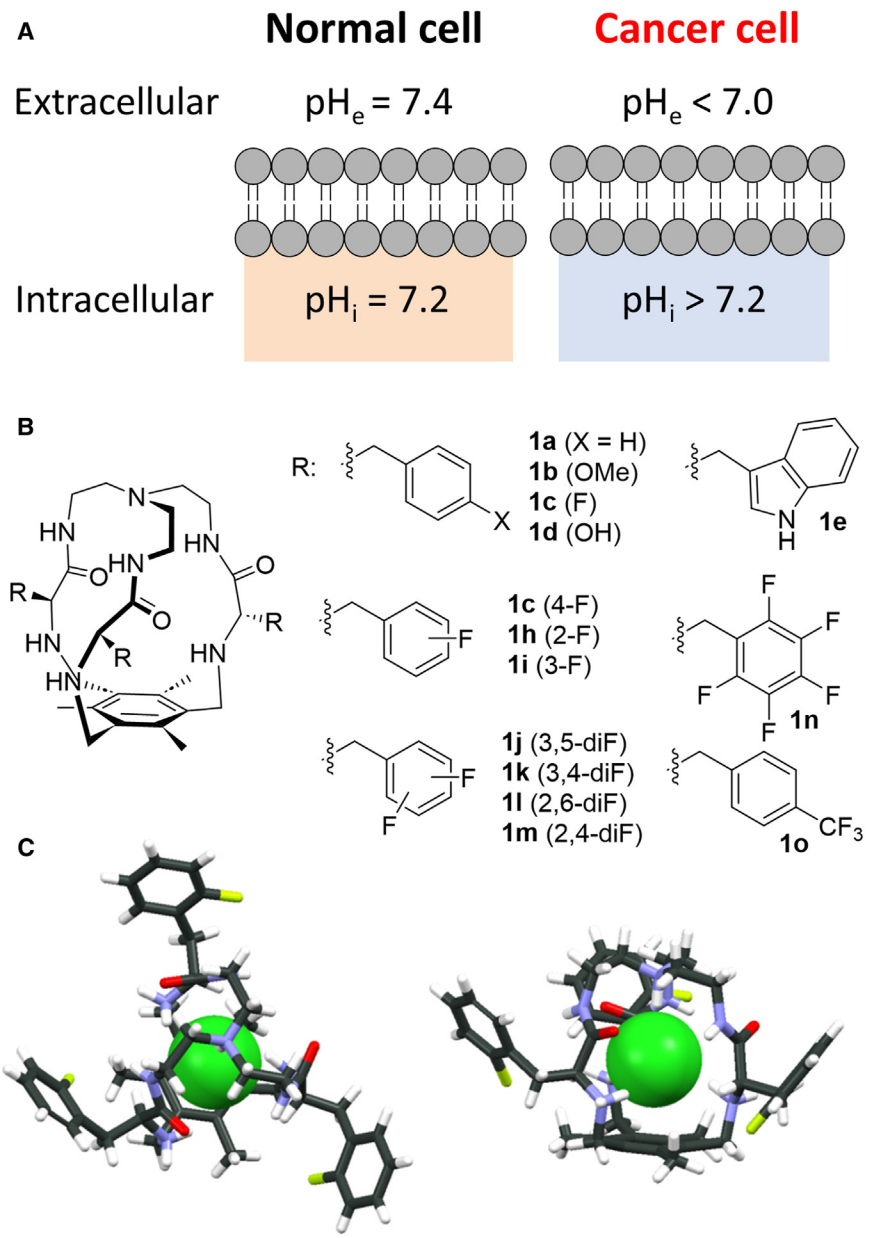

Figure 1. Biological and chemical background

(A) Reversal of extra-/intracellular pH gradient in cancer cells.

(B) Chemical structures of the pseudopeptidic cages.

(C) X-ray diffraction results of the crystals of the tetra-HCl salt of cage **1h**. The chloride included in the cage cavity is shown as a green space-filling sphere. Solvent molecules and additional chloride anions in **1h**·4HCl are omitted for clarity.

microenvironment.[32] Additionally, in many cases, and especially for anion transport, the ion influx/efflux is strongly coupled to proton transport.[33–41] According to these facts, there is room for implementing selectivity in anion transporters to selectively kill cancer cells by making an anionophore work more efficiently in slightly acidic microenvironments.[12,42–46] This relatively simple idea is difficult to translate into specific chemical entities.[41,47] In most cases, the difference in pH required to display measurable anion transport differences leading to clear-cut on-off biological activity is larger[48–56] than those observed in cancer cell biology.[57] Moreover, the actual

anion transport mechanism of synthetic ionophores through cell membranes is a complex process at the molecular level, depending on many interconnected factors still not fully understood.[27,58–60] In this regard, we have previously reported small tripodal pseudopeptidic cages[61] that strongly encapsulate a chloride anion when their amine groups are protonated.[62] These cages efficiently transport chloride through lipid bilayers by a H^+/Cl^- symport mechanism,[63] with a more efficient transport at slightly acidic pH.[64] This pH-dependent HCl transport nicely correlates with pH-dependent cytotoxicity against cancer cells with pH-switching values close to those found in cancer biology.[64] The most selective cage was the one derived from 4-F-phenylalanine amino acid (**1c** in Figure 1B), suggesting that fluorine substitution could subtly modulate the physicochemical properties of the cages (basicity, chloride binding, lipophilicity, diffusiveness, chloride exchange rate, etc.) with a strong impact on their biological activity.[65,66] Actually, fluorine is a very peculiar element: its small size, high electronegativity, and hydrophobicity has promoted the development of fluorine-substituted molecules for studies at the chemistry-biology interface.[67,68] Besides, ^{18}F is a radioisotope widely used for labeling radiopharmaceuticals.[69,70] Moreover, endogenous fluorinated organic compounds are absent, making fluorine substitution a very popular process in medicinal chemistry and chemical biology.[71,72] In the current study, we have systematically studied the effect of fluorine substitution on the pseudopeptidic cages (Figure 1B) in order to better understand the process at the molecular level. Besides, we have unraveled the impact of the structural factors on the biological activity, allowing the identification of a more pH-selective cytotoxic cage with very promising *in cellulo* anti-cancer activity.

RESULTS AND DISCUSSION

Design and synthesis of the pseudopeptidic cages

Taking into account our previous results[64] with a pseudopeptidic cage derived from 4-F-phenylalanine (**1c** in Figure 1B), we decided to systematically test the effect of an increasing number of fluorine substitutions on the aromatic residues (**1c** and **1h–1o**). Also, the position of the F atoms was considered to be an important structural parameter (**1c**, **1h**, **1i**, and **1j–1m**, respectively). With this in mind, we synthesized molecules **1h–1o** to compare with the previously described **1c**. The syntheses of the cages were carried out following slight variations of our reported procedure, for which the key macrobicyclization step is a chloride-templated triple nucleophilic substitution.[62–64] In all cases, the molecules were obtained with good yields after purification and characterized using standard spectroscopic (nuclear magnetic resonance [NMR], electrospray ionization mass spectrometry [ESI-MS]) and analytical (high-performance liquid chromatography [HPLC]) techniques (see details in the supplemental information).

Chloride binding

When protonated, the tripodal pseudopeptidic cages strongly bind chloride.[62–64] We performed ^1H NMR titration experiments of the fully protonated cages with tetrabutylammonium chloride (TBACl) in 5% aqueous deuterated acetonitrile to study the effect of the fluorine substitution on chloride recognition. Since complexes with 1:2 cage:chloride stoichiometry were detected in some cases, we used the BC_{50}° parameter[73] to compare the binding efficiency (Table 1). The fitting of the NMR titration data shows that chloride recognition is only slightly affected by the position of the fluorine atom at the side chains (entries 1–3 in Table 1) or even the presence of two fluorine atoms at each residue (entries 6 and 7 in Table 1). These results agree with a conserved binding site for chloride at the inner cavity of the cage. A further demonstration was obtained by X-ray diffraction of the single crystal of **1h**·4HCl,

Table 1. Properties of the fluorinated pseudopeptidic cages

Entry	Cage	Logβ_1[a] [Logβ_2]	$BC_{50}°$ (μM)[b]	cLogP[c]	t_R (min)[d]	J_0 pH/s[e]	CC_{50} (μM)[f] pH 6.2	CC_{50} (μM)[f] pH 7.2	CC_{50} (μM)[f] pH 7.5
1	**1c** (4-F)	3.82(3) [6.0(1)]	148 ± 5	4.00	9.44	0.02354	29 ± 4	58 ± 10	166 ± 35
2	**1h** (2-F)	3.75(9)	173 ± 4	4.00	8.02	0.02773	14 ± 2	17 ± 3	13 ± 2
3	**1i** (3-F)	4.4(1) [6.5(2)]	36 ± 8	4.00	9.22	0.02280	13 ± 3	~25	~25
4	**1j** (3,5-diF)	n.m.	n.m.	4.38	10.64	0.01498	n.m.	n.m.	>200
5	**1k** (3,4-diF)	n.m.	n.m.	4.39	10.33	0.01472	~100	>200	>200
6	**1l** (2,6-diF)	4.3(2)	50 ± 15	4.37	8.28	0.02076	17 ± 2	18 ± 2	14 ± 2
7	**1m** (2,4-diF)	4.3(2)	50 ± 15	4.38	9.53	0.02612	25 ± 8	62 ± 10	≥200
8	**1n** (F_5)	n.m.	n.m.	5.51	13.07	0.00904	n.m.	n.m.	>200
9	**1o** (4-CF_3)	n.m.	n.m.	5.90	12.44	0.01053	>200	≥200	≥200

n.m., not measured.

[a]Chloride binding stability constants (Logβ_n, ^{1}H NMR titration in 95:5 CD_3CN:H_2O, values in parenthesis are the standard deviations in the last significant figure; see Figures S2–S9).

[b]Affinity ($BC_{50}°$).

[c]Calculated lipophilicity (cLogP).

[d]Experimental lipophilicity (t_R in reverse-phase HPLC).

[e]pH gradient dissipation through lipid bilayers (initial transport rate measured with the HPTS fluorescent probe, Table S2; Figures S15–S23).

[f]A549 cytotoxic concentration for 50% cell viability (CC_{50} by MTT assay, Figures S44–S51) at different pH values.

which confirmed the conservation of the chloride binding site through H-bonding and ionic interactions with the corresponding protonated amines (Figure 1C). Actually, the comparison of the crystal structures of **1h** with those of **1a**,[62,63] **1b**,[64] and **1d**[64] showed high structural similarity (Figure S1), reflecting a close resemblance in the chloride recognition properties.

Physicochemical properties: Protonation and lipophilicity

Protonation state and lipophilicity are two key physicochemical parameters of anionophores since they define their behavior at the lipid/aqueous interphase. Moreover, for the cages described here, the protonation state will also dictate the chloride affinity and exchange rate, as these are generally more efficient for protonated species.[62–64] Thus, we decided to study the effect of peripheral F substitutions on the basicity of the amine groups of the cages. The low solubility of the free amines in pure water precluded the determination of the corresponding pK_a values by potentiometric pH titrations. However, we realized that the fluorescence emission spectra of the molecules are strongly affected by the pH of the medium, allowing the estimation of the corresponding apparent pK_a values in a water/methanol mixture. The fluorescence pH titrations were done with cages bearing F atoms at positions 2 (**1h**), 3 (**1i**), and 4 (**1c**) of the aromatic side chains. Also, the Phe cage (**1a**)[62,63] lacking fluorine atoms was measured as the reference compound. Global fitting of the emission spectra at different pH rendered the corresponding pK_a values (Table 2; Figure S10) that allow the determination of the species distribution vs. the pH (Figure 2A). A convenient way to compare the molecules is to plot the average protonation state as a function of the pH for each cage (Figure 2B). Several important trends can be extracted. The effect of the fluorine substitutions is more important in the two first protonation steps (compare traces at pH > 8 in Figure 2B), being the main difference in the second pK_a (Table 2). We can hypothesize that the first protonation takes place in the tertiary amine (very similar in all cases), while the second protonation must occur in one of the secondary amines from the amino acidic moieties. The lower basicity of the secondary amine in the fluorinated cages can be explained by the electron-withdrawing inductive effect of the fluorine atoms in the side chains. However, further protonation is similar for all the cages except **1h**, which shows more basic amines for the third and fourth consecutive protonation steps

Table 2. Protonation constants of pseudopeptidic cages

Entry	Cage	pK_{a1}	pK_{a2}	pK_{a3}	pK_{a4}
1	**1a** (H)	10.13(2)	10.1(1)	6.7(1)	4.6(1)
2	**1h** (2-F)	9.69(2)	8.68(4)	7.03(6)	6.5(1)
3	**1i** (3-F)	10.24(5)	7.8(1)	6.6(1)	4.7(1)
4	**1c** (4-F)	10.01(3)	8.0(1)	6.7(2)	4.2(2)

Protonation constants of pseudopeptidic cages were determined by fluorescence pH titrations in 3:2 H_2O:MeOH solutions. Values in parentheses are the standard deviation in the last significant figure.

(Table 2; Figure 2B, with the red trace well above the others at pH < 8). Rather counterintuitively, the *ortho* F substitution in the side chains of **1h** stabilizes the protonation at the secondary amines. A conformational analysis of the **1h**·HCl complex (Figure 2C; see also the supplemental information) showed the possible formation of intramolecular H-bonds between the F atom and the NH of the secondary amine or amide groups of the contiguous arms of the cage.[74] These interactions would enhance the basicity of the secondary amine and also produce more folded conformations in solution (see below). Overall, the *ortho* F substitution leads to a more protonated and more compact structure at pH values between 6 and 8, which might be especially important for the biophysical and biological assays.

Regarding the lipophilicity, the theoretically calculated partition coefficients (cLogP, Table 1) do not reflect the large differences observed experimentally by reverse-phase HPLC (retention times in Table 1) for fluorinated isomers. The larger number of fluorine atoms increases lipophilicity, an expected general trend and also well established by cLogP. However, there is a clear dependence on the position of the F atom that is not satisfactorily predicted by cLogP. Thus, the *ortho* F substitution makes **1h** much more hydrophilic (compare entry 2 with entries 1 and 3 in Table 1), and this is retained for **1m** (entry 7 vs. 4 and 5) and especially for **1l** (entry 6 vs. 4 and 5). Since the HPLC experiments were carried out at pH 2, full protonation of all the cages is expected (Figure 2B). The observed differences can be reasonably explained considering that the F substitution at position 2 of the side chain produces a more folded conformation (as previously supported by molecular modeling) that precludes the interaction of the aromatic side chains with the hydrophobic stationary phase, rendering a lower retention. The cages **1j**, **1k** (two F per side chain, one of them at position 3) and **1n**, **1o** (three or more F atoms per residue) are very hydrophobic, proving troublesome for both the ^{1}H NMR titration experiments and the biological assays (see below).

Chloride transport at the aqueous-lipid interphase

In order to test the anionophoric activities of the synthesized cages, we used a fluorescence emission test with 8-hydroxypyrene-1,3,6-trisulfonic acid (HPTS),[75] which measures pH variations with high sensitivity. Previous studies showed that these cages co-transport HCl through lipid bilayers,[63] as this property is closely related to their biological activity.[64] Thus, 1-palmitoyl-2-oleoyl-sn-glycero-3-phosphocoline (POPC) vesicles were loaded with a $NaNO_3$/NaCl aqueous solution (123.9 mM $NaNO_3$, 10 mM NaCl, 10 mM NaH_2PO_4, ionic strength [I.S.] 150 mM, pH 6.5) and the HPTS (1 mM) fluorescent probe. These vesicles were suspended in a medium with identical ionic composition but lacking the HPTS and at a more basic pH (7.5). These conditions were chosen to mimic a biorelevant pH gradient window. Addition of the cages produces a rise of the intravesicular pH that can be readily measured by the HPTS emission properties (see the supplemental information for details). The time dependence of the intravesicular pH for all the synthesized cages is plotted in Figure 3. For comparative purposes, the initial rate of pH changes

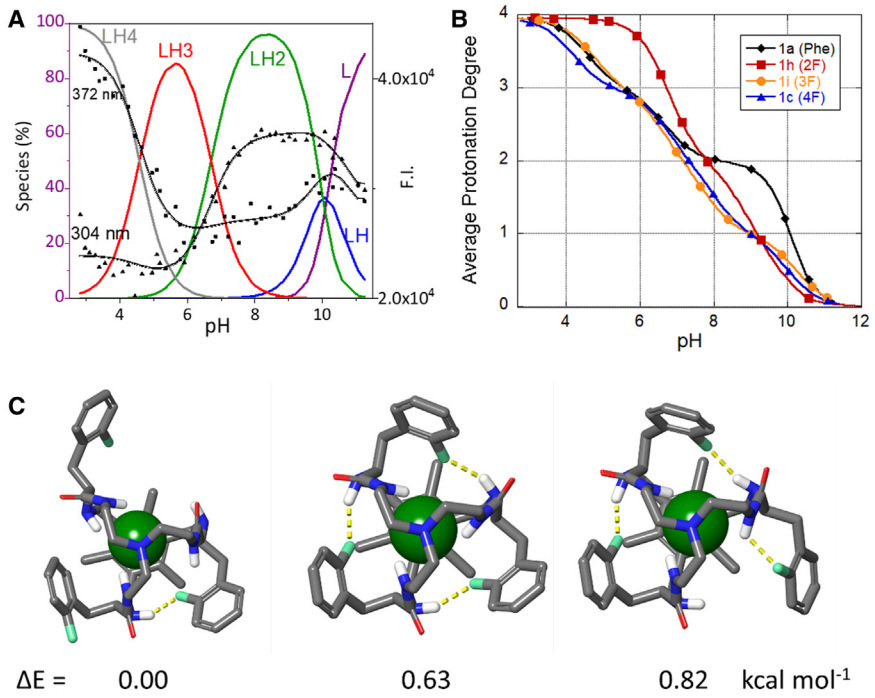

Figure 2. Protonation of pseudopeptidic cages

(A) Representative protonation species distribution (left axis) and fluorescence emission (right axis) at two wavelengths vs. pH values for **1a** (the rest are given in the supplemental information, Figure S10).

(B) Plot of the average protonation states vs. pH calculated from the corresponding pK_a values.

(C) Lowest energy DFT-optimized (B3LYP-D3/6-31G** level with PBF implicit water solvation) conformations determined for the **1h**·HCl complex, highlighting in yellow the possible H-bonds implicating fluorine from the aromatic side chain.

induced by the cages was determined for all compounds. This value, defined as J_0 (pH/s), is included in Table 1. Compounds **1h** and **1m**, bearing 2-F and 2,4-diF aromatic substituents, were found to be the most active in these assays, whereas compounds **1j**, **1k**, **1n**, and **1o** were found to be the least efficient at discharging the pH gradient. Within the series of compounds evaluated, a negative correlation between the lipophilicity of the compounds and the activity in these assays was observed, suggesting that the increase of the hydrophobicity (number of F atoms, especially in certain positions of the aromatic side chains) is detrimental for the ionophoric activity. Control experiments with carboxyfluorescein ruled out the formation of large pores by the action of the cages (Figure S24).

We wanted to obtain a more detailed molecular picture of the ionophores at the aqueous-lipid interphase. To this aim, we performed ^{1}H NMR experiments of the cages in deuterated dodecylphosphocholine (DPC) micelles suspended in pure D_2O at different pH and ionic strength values.[64] These experiments give us information about the incorporation of the cages within the lipid phase, their conformational characteristics, and the chloride binding and exchange processes. Thus, the cages could be in dynamic equilibrium in/out of the micelles, and chloride could also be included within the cage in any of the two phases (Figure 4A). The proposed equilibria will be modulated by the chloride affinity and lipophilicity of the cages, also determined by their protonation degree and conformation. The first intriguing observation is the different appearance of the aromatic proton signals for **1c** (4-F) and **1h** (2-F). As we have previously shown,[64] **1c** was included inside the micelles exchanging the chloride anion with the aqueous phase at a slow rate in the NMR

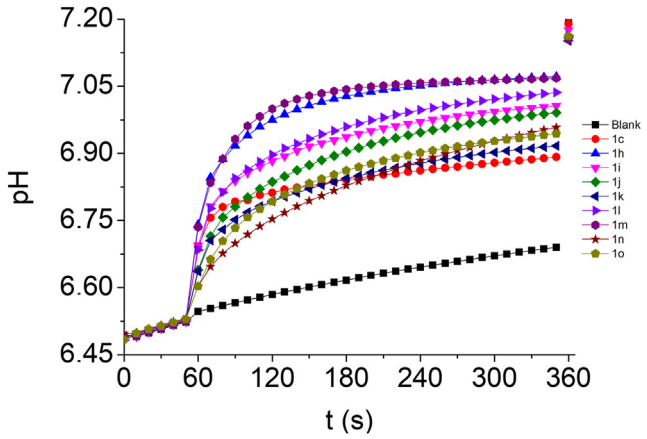

Figure 3. Plot of the intravesicular pH

Measured with HPTS fluorescent probe as a function of time upon addition of different cages (50 μM: 10% mol carrier to lipid concentration; initial pH 6.5 inside the vesicles, suspended in aqueous buffer at pH 7.5).

chemical shift timescale (Figure 4B). For **1c** at acidic pH, the chloride binding increased, and the exchange rate was much faster, explaining its pH-dependent performance as an ionophore. However, the cage with F in the *ortho* position (**1h**) shows a single set of signals in all tested conditions, implying a fast exchange in the NMR chemical shift timescale. Moreover, the external acidic pH produces a more pronounced chemical shift perturbation in the aromatic signals of **1h**, which are further perturbed upon the addition of NaCl (Figure 4B). The downfield shifts of H3 and H4 are especially noteworthy, suggesting that the side chains are somehow implicated in the dynamic process. The nuclear Overhauser effect spectroscopy (NOESY) spectrum of **1h** in the micelles at acidic pH is depicted in Figure 4C, which shows strong cross-peaks between the aromatic protons and the core of the cage (both the tris(2-aminoethyl)amine [TREN] moiety and the Me signals, blue double-headed arrows in Figure 4C). Especially remarkable are those implying H6 and H5, which strongly suggests a very compact conformation with the side chains folded toward the cage core (Figure 4C). This is in very good agreement with the reduced hydrophobicity of **1h** observed experimentally by reversed-phase HPLC and can be explained with the H-bonding interactions proposed from the theoretical models and also depicted in Figure 4C as red dashed lines.

The relative incorporation of the cages within the lipid phase is also an important factor. This can be accurately measured by diffusion-ordered spectroscopy (DOSY) experiments: the comparison between the self-diffusion rates (D) of the lipid (measured with the residual protonated methylene signals of deuterated DPC) and the cage serves as a suitable parameter in this regard. One should bear in mind that the DPC micelle is in dynamic exchange with DPC monomers in solution, and the observed D(DPC) is a weighted average of those of the monomer and micelle. A relative diffusivity (expressed as D(cage)/D(DPC), see Figure 4D) lower than one implies a larger apparent size of the cage and, therefore, the major inclusion of the cage inside the micelles. As the relative diffusivity increases, the leaking of the cages to the aqueous phase also increases. Figure 4D shows a plot of the obtained diffusivity for two isomeric fluorinated cages (**1c** and **1h**) and that from Phe (**1a**) as a reference. At neutral pH both in the absence and the presence of salt, the three cages mainly remain in the micelles. At acidic pH, we observed a differential behavior: **1a** starts leaking to the aqueous phase, while both

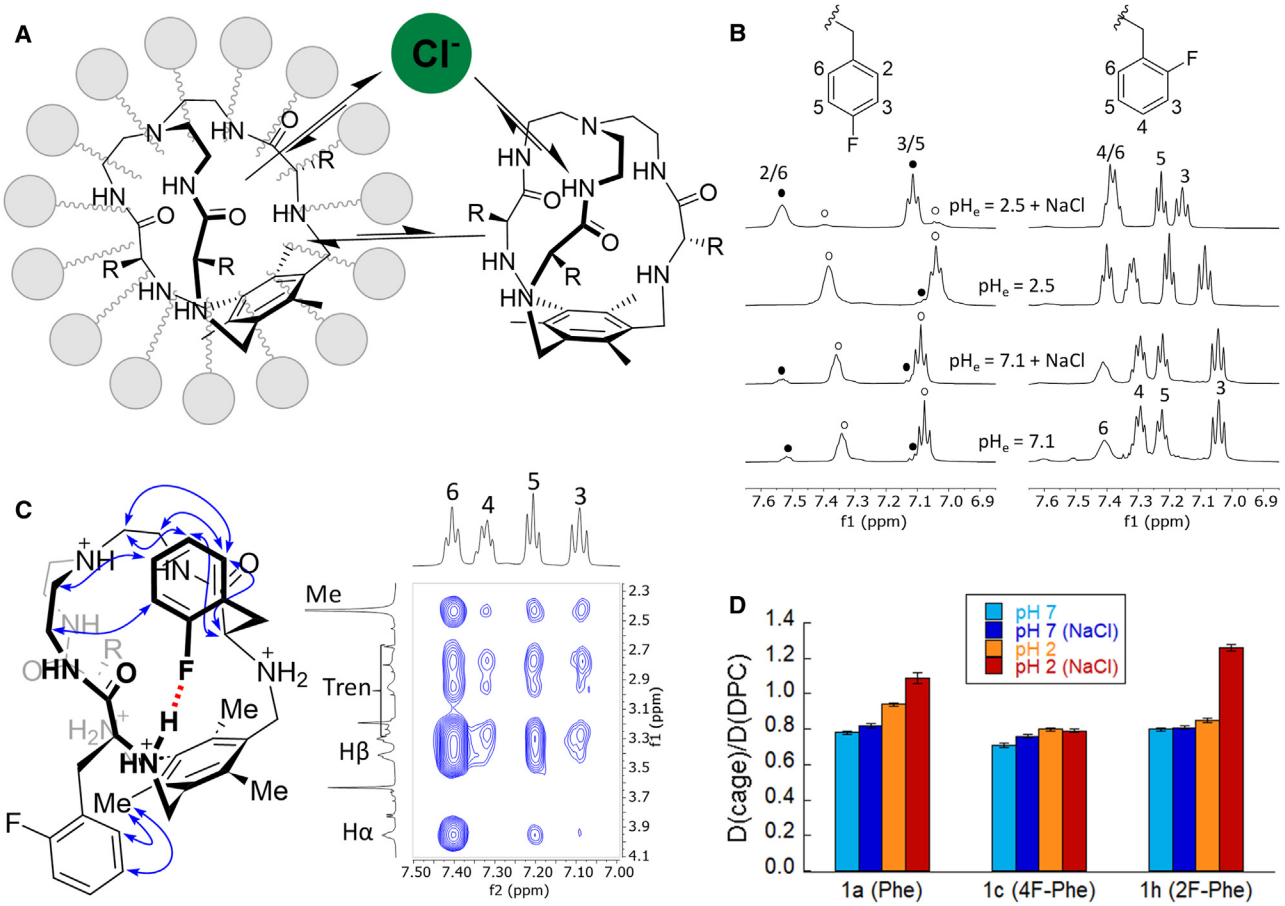

Figure 4. NMR experiments in deuterated DPC micelles suspended in water

(A) Schematic representation of the possible exchange mechanisms between the cage, micelle, and chloride anion.

(B) Aromatic ^{1}H NMR region for **1c** (left) and **1h** (right) at different pH and ionic strength (empty and filled circles show signals from free and chloride-complexed **1c** in slow exchange).

(C) Selected region of the 2D NOESY spectrum performed with **1h** in DPC micelles at acidic pH. The highlighted NOE cross-peaks are shown as blue double-headed arrows in the chemical structure, while the proposed H-bonding interactions are depicted as red dashed lines.

(D) Plot of the relative diffusivity (D(cage)/D(DPC)) of **1a**, **1c**, and **1h** in DPC micelles under different aqueous conditions (pH and presence of added NaCl). Error bars show standard deviation from the fitting to extract D values.

fluorinated cages mainly remain inside the micelles. This behavior suggests that fluorine favors the inclusion in the lipid phase, as expected. The addition of NaCl at acidic pH induces the leaking of **1a** (Phe) and **1h** (2F-Phe) but not of **1c** (4F-Phe). This implies that different possible exchange mechanisms can be operating depending on the cage, the pH, and the presence of salt. Thus, **1h** mainly differs from **1c** in a higher trend to be transferred to the aqueous phase at low pH and in the presence of salt, suggesting that in these conditions, the cage can exchange in and out of the micelles. This correlates with its lower lipophilicity and more compact conformation. However, **1c** remains in the lipid phase regardless of the pH and ionic strength of the aqueous phase. Overall, all the data point to the higher polarity and mobility of **1h**, which is also reflected in a faster chloride exchange (as observed by NMR). Our results also show that **1h** remains within the micelles at neutral pH despite its higher apparent average basicity (see Figure 2C). Therefore, under these conditions, an in/out chloride exchange mechanism must also be operating for the 2F-Phe cage.

Molecular modeling of the transport process through lipid bilayers mimicking cell membranes

Molecular dynamics simulations were performed to investigate the interaction and translocation of pseudopeptidic cages across a model POPC lipid bilayer. Thus, compounds **1c** and **1h** were simulated in (1) a neutral and free state or (2) monoprotonated and complexed with a chloride anion, and both with initial locations either in the bulk water (W) or the middle of the lipid bilayer (M). When complexed with chloride, restraints were needed to prevent dissociation. Collectively, the results obtained (full description in the supplemental information) showed that the free diffusion of the cages into the lipid membrane led to stabilization around 5–10 Å below the membrane surface, regardless of their initial placement or charge state. This finding suggests that the most stable location for these cages, whether free or complexed, is within the membrane near the water-lipid interface, which facilitates their role as anion transporters. These computational results are in agreement with the experimental observations by NMR in DPC micelles with paramagnetic labels (Figure S42).

To explore the energetic barriers involved in the process of membrane crossing, the potential of mean force (PMF) profiles for **1c** and **1h**, both free and HCl bound, were calculated by combining umbrella sampling (US) simulations with the weighted histogram analysis method.[76,77] The PMF profile for the crossing of a free chloride anion was also computed for comparison purposes. To that end, steered molecular dynamics simulations were first conducted to generate starting positions along the normal of the membrane. Two approaches were considered: pulling the cages from the middle of the membrane to the water phase on both sides or pulling the cages from the water phase across the membrane. The first option was chosen to avoid potential problems, and up to three series of US simulations were conducted in each direction (Figure 5A; supplemental information). The results showed acceptable reproducibility among the three profiles in each direction. Furthermore, to depict the real PMF profile accurately, the six individual profiles for each case were averaged, assuming symmetry (Figure 5B). This cumulative sampling represented almost 2 μs for each cage.

According to the PMF profiles in Figure 5B, the crossing of a single chloride anion through the model membrane exhibits an energetic barrier of about 21 kcal mol^{-1} at Z = 0, aligning reasonably with previously reported data.[76] This barrier disappears for the chloride complexes of monoprotonated **1c** and **1h**. Interestingly, the PMF profiles for both complexes are nearly identical, suggesting comparable chloride transport capacities. However, the PMF profiles of neutral and free **1c** and **1h** show remarkable differences among themselves and compared to their complexed forms. Despite the fact that both **1c** and **1h** exhibit energy minima at Z = $\pm$10 Å, these minima are deeper for **1c** (−16 vs. −11 kcal mol^{-1}). The lower energy values for free **1c** compared to free **1h** suggest that the former is more stabilized in the lipid environment, consistent with the experimentally observed differences in lipophilicity. Additionally, the disparities observed between free **1c** and **1h** suggest that **1c** faces a higher energy barrier compared to **1h** to reach the water phase, or the membrane surface, from its preferred location within the membrane. This could explain the anion transport capacities of both compounds and is in very good agreement with the DOSY results for their behavior in the DPC lipid-water interphase.

Formally, chloride transport can be conceptualized as a two-step cycle: first, the translation of the chloride-bound protonated cage across the membrane, releasing the anion and a proton to maintain charge neutrality, and second, the return of the

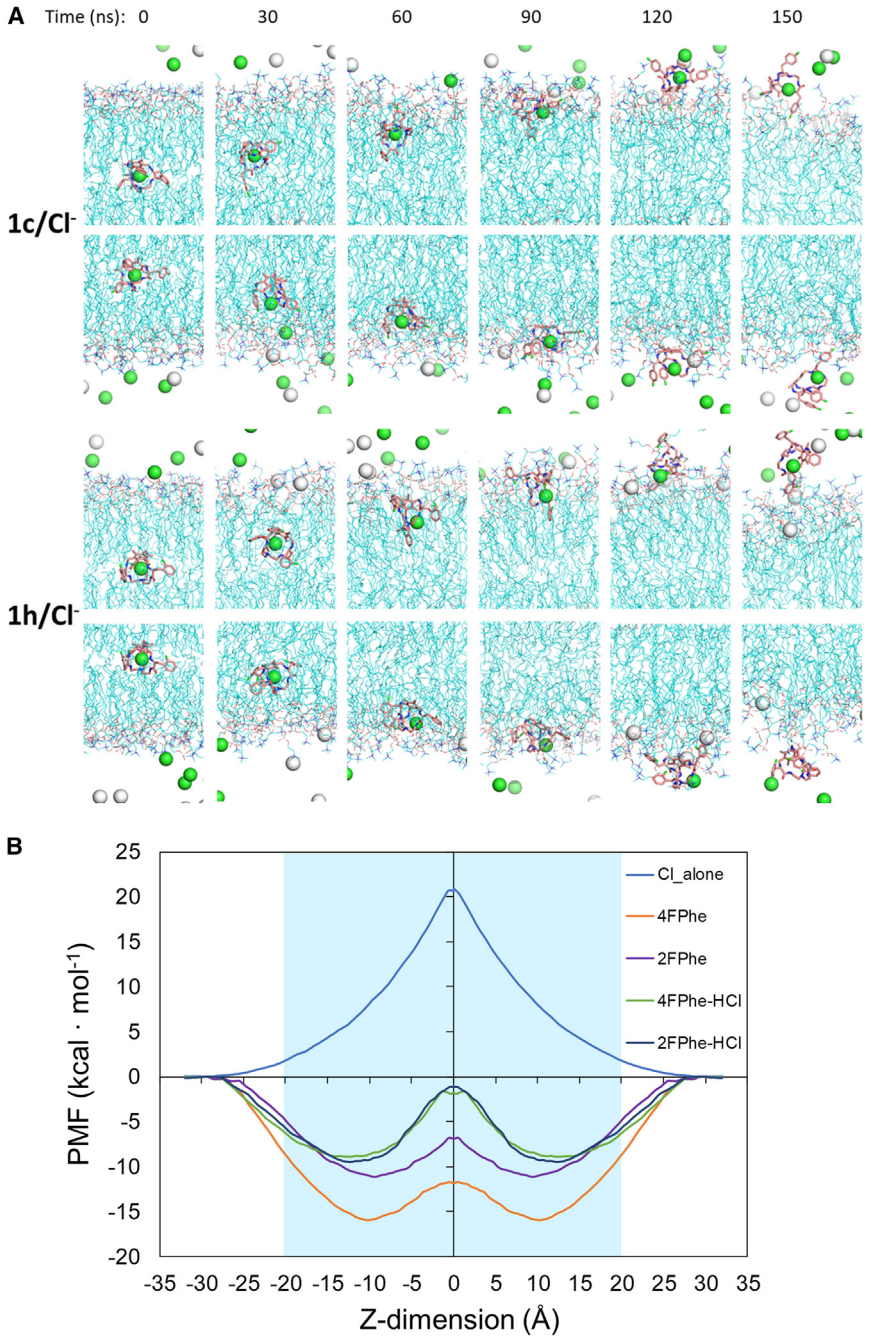

Figure 5. Molecular dynamics simulations

(A) Snapshots of representative steered molecular dynamics simulations of chloride-bound monoprotonated **1c** and **1h** used to generate the starting positions along the normal of the membrane for the US simulations.

(B) PMF graphs resulting from averaging the results of 6 independent US series (see the supplemental information). Free chloride anion (blue), **1c** (orange), **1h** (purple), and the chloride complexes of monoprotonated **1c** (green) and **1h** (black). The blue shaded region corresponds to the lipid bilayer.

neutral cage to undergo reprotonation and load a new anion, restarting the cycle. Therefore, the above results suggest that although the first step of the cycle is energetically similar for both **1c** and **1h**, the second step may be more kinetically favorable for **1h**, consistent with the observed transport rates for each cage (Table 1).

Analysis of cage geometry during the US simulations (see the supplemental information) shows that **1c** tends to adopt semi-extended conformations, while **1h** assumes more folded conformations, correlating with the observed NOEs in lipid micelles (Figure 4C). The folded conformations in **1h** could reduce the possibility of establishing hydrophobic interactions with the membrane, while the unfolded conformations in **1c** may enhance them, explaining the energetic differences in the PMF profiles. On the other hand, the chloride complexes of both cages predominantly exhibit extended conformations, likely due to the electrostatic repulsion between the chloride and the aromatic side rings. Although this could stabilize the cages through hydrophobic interactions with the lipids, this stabilization could be overcompensated by the lower stability of a charged complex in a hydrophobic environment, which would explain the higher energy PMF profiles.

pH-dependent cancer cell cytotoxicity

We studied the cytotoxicity (MTT assay) of all the fluorinated cages toward human lung adenocarcinoma cells (A549) using different external pH conditions to mimic the acidic microenvironment of solid tumors. In all cases, the cell viability was determined with suitable control experiments performed at the corresponding pH values in the absence of the cages. Marked differences were observed when comparing cages with different numbers and dispositions of the F atoms in the side chains (Table 1; Figures S44–S51). The cages with high numbers of fluorine atoms (**1n** and **1o**), as well as those bearing two fluorine atoms per side chain with one of them at position 3 (**1j** and **1k**), showed no or very low cytotoxicity at all the pH conditions tested (Table 1). These results correlate well with the liposome-based assays, as these compounds were also found to be the least efficient in the HPTS assay. When comparing cages bearing one F per side chain, the results are strikingly different. Thus, although the three cages are cytotoxic, only **1c** shows a clearly pH-dependent CC_{50} (Table 1, entry 1). Cage **1h** is very active at all the pH values tested here (Table 1, entry 2), with very similar CC_{50} values. The different behaviors between **1c** and **1h** can be explained considering their different physicochemical properties. Thus, at pH 7.5, **1c** has, on average, less than two protonated amines, being diprotonated at pH < 7 (Figure 2B). On the contrary, **1h** bears more than two protons, on average, in the whole pH range tested here. The case of **1i** is more difficult to rationalize since the cell viability curves did not reach complete cell killing (Figure S45), most likely due to solubility issues, especially at pH 7.5. The higher protonation degree and faster chloride exchange with host **1h** at neutral pH effectively produce a more cytotoxic ionophore. On the other hand, the change in the protonation degree of **1c** around pH 7 accounts for the observed pH-dependent cytotoxicity. When comparing the cages bearing two F atoms per side chain with two *ortho* (**1l**) or *ortho*/*para* (**1m**) positions, the trends are remarkable (Figure 6A). Thus, despite being isomers with the same chloride affinity (Table 1), **1l** shows a pH-independent high cytotoxicity (dashed lines in Figure 6A and entry 6 in Table 1), while **1m** shows a marked pH-dependent cell toxicity (solid lines in Figure 6A and entry 7 in Table 1), which is even more pronounced than that exhibited by **1c** (Figure 6B). Thus, cage **1m** is essentially non-toxic (CC_{50} > 200 μM) at pH 7.5, a pH expected around healthy cells, but very toxic in a slightly acidic medium like the one found in tumor microenvironments. Thus, as a general conclusion, the *ortho* F substitution (**1h** and **1l**) increases cytotoxicity, while the *para* F substitution (**1c**) implements the pH-dependent selectivity. Very remarkably, the effects are somehow accumulative since the cage bearing *ortho*/*para* disubstitution (**1m**) is both highly toxic and pH selective. Moreover, we rationalized the cytotoxicity switch of **1c** around pH 7 as a consequence of the change in the protonation state (Figure 2B). Accordingly, we hypothesized that the *ortho*-substituted

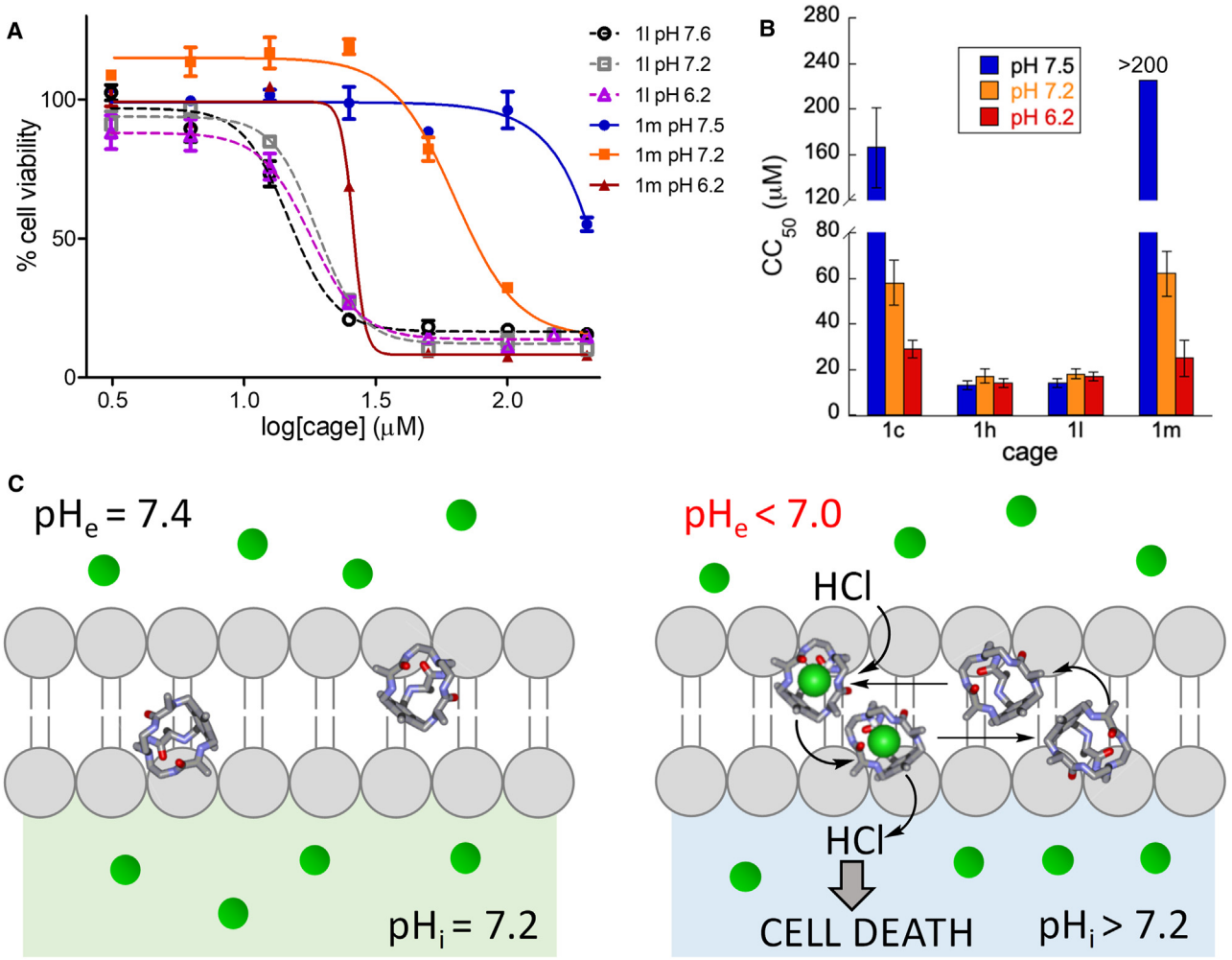

Figure 6. Biological activity of pseudopeptidic cages

(A) A549 cell viability (% by MTT assay) as a function of the cage concentration at different pH values for **1l** (2,6-diF-Phe, empty symbols and dashed lines) and **1m** (2,4-diF-Phe, solid symbols and lines). Each trace corresponds to an average of at least three independent experiments. For the other cages, see Figures S44–S51.

(B) Plot of the CC_{50} values for some selected cages.

(C) Schematic representation of the proposed mechanism for the pH-modulated cell toxicity mediated by the pseudopeptidic cages.

Error bars in (A) and (B) correspond to standard deviation from the replicates.

cages would experience a similar cytotoxicity switch at pH > 8, where the average protonation degree is lower than two. The MTT assays at pH 8.0 and 8.5 for **1h** and **1l** showed low toxicity (Figures S52 and S53), thus confirming our hypothesis and the key role of the protonation degree and ionophoric properties in the biological activity of the cages (Figure 6C).

We have also performed preliminary cell toxicity studies with spheroids, which are proposed as an intermediate stage between cell culture and tissues. Remarkably, two of the cages (**1c** and **1h**) showed cell viability trends in spheroids of A549 cells similar to those obtained in conventional MTT assays in cell plates (Figures S54 and S55). These results nicely support the possibility of designing an active ionophore that displays cytotoxicity selectively under pH conditions characteristic of tumor microenvironments.

Accordingly, we have shown that the low selectivity of synthetic anionophores for cancer chemotherapy can be overcome by taking advantage of the acidic microenvironment of solid tumors. However, the narrow pH range for the necessary toxicity switch requires a very delicate tuning of the physicochemical properties of the target molecules. In this work, we have unraveled the intriguing effect of peripheral fluorine substitution on the biological activity of synthetic small pseudopeptidic cages derived from phenylalanine. The number and position of the F atoms on the aromatic side chains strongly impact key physicochemical properties like basicity, lipophilicity, and chloride exchange, as well as conformational and diffusional properties at the water-lipid interphase, which finally define the ionophoric activity and pH-dependent cytotoxicity. As a rule of thumb, the F substitution at position 2 of the aromatic side chain increases cytotoxicity, while fluorine at position 4 implements a pH-dependent activity switch that is close to the target values (pH = 6.0–7.5). The effect is remarkably additive since the corresponding cage bearing 2,4-difluoro-substituted aromatic side chains shows optimal pH-modulated cytotoxicity for killing cancer cells in an acidic local microenvironment, leaving the cells in normal pH unaffected with a wide (ca. 10-fold) concentration range. Besides the definitive demonstration of the concept, we have proposed a reasonable structural explanation supported by experimental data and theoretical models. The conclusions extracted here will facilitate future designs of improved ionophores for biological applications in cancer and also for other serious diseases related to anion transport.

EXPERIMENTAL PROCEDURES

Resource availability

Lead contact

Further information and requests for resources should be directed to and will be fulfilled by the lead contact, Ignacio Alfonso (ignacio.alfonso@iqac.csic.es).

Materials availability

All materials generated in this study are available from the lead contact upon reasonable request.

Data and code availability

All of the data supporting this study have been shown in the article and supplemental information. Other related data are available from the corresponding authors upon reasonable request.

The X-ray diffraction results for **1h**•4HCl crystals were deposited in the Cambridge Crystallographic Data Center with the specific code CCDC 2182742. This can be accessed at https://www.ccdc.cam.ac.uk/ with the corresponding code.

SUPPLEMENTAL INFORMATION

Supplemental information can be found online at https://doi.org/10.1016/j.xcrp.2024.102152.

ACKNOWLEDGMENTS

We are thankful for the funding from the Spanish Research Agency of the Spanish Ministry of Science, Innovation and Universities MICIU/AEI/10.13039/501100011033 (grants PID2021-128411NB-I00 and PID2020-117610RB-I00) and the European Social Fund. The authors gratefully acknowledge the computational resources of the Consorci de Serveis Universitaris de Catalunya (CSUC) and Centro

de Supercomputación de Galicia (CESGA), as well as Andrea Sancho-Medina for her contributions to transmembrane anion transport experiments.

AUTHOR CONTRIBUTIONS

L.T., Y.P., I.C.-B., M.B., C.B., and J.S. conducted the experiments; J.B. designed and conducted the molecular modeling; Y.P., J.S., R.Q., and I.A. designed the experiments; I.A. conceptualized and supervised the project; I.A. wrote the first draft; and all authors read, edited, and approved the final version of the manuscript.

DECLARATION OF INTERESTS

The authors declare no competing interests.

Received: May 23, 2024
Revised: July 11, 2024
Accepted: July 19, 2024
Published: September 3, 2024

REFERENCES

1. Sung, H., Ferlay, J., Siegel, R.L., Laversanne, M., Soerjomataram, I., Jemal, A., and Bray, F. (2021). Global Cancer Statistics 2020: GLOBOCAN Estimates of Incidence and Mortality Worldwide for 36 Cancers in 185 Countries. CA A Cancer J. Clin. *71*, 209–249. https://doi.org/10.3322/caac.21660.

2. Bray, F., Laversanne, M., Weiderpass, E., and Soerjomataram, I. (2021). The ever-increasing importance of cancer as a leading cause of premature death worldwide. Cancer *127*, 3029–3030. https://doi.org/10.1002/cncr.33587.

3. Costa, A.F., Campos, D., Reis, C.A., and Gomes, C. (2020). Targeting Glycosylation: A New Road for Cancer Drug Discovery. Trends Cancer *6*, 757–766. https://doi.org/10.1016/j.trecan.2020.04.002.

4. Dembic, Z. (2020). Antitumor Drugs and Their Targets. Molecules *25*, 5776. https://doi.org/10.3390/molecules25235776.

5. Farkona, S., Diamandis, E.P., and Blasutig, I.M. (2016). Cancer immunotherapy: the beginning of the end of cancer? BMC Med. *14*, 73. https://doi.org/10.1186/s12916-016-0623-5.

6. Cheng, Z., Li, M., Dey, R., and Chen, Y. (2021). Nanomaterials for cancer therapy: current progress and perspectives. J. Hematol. Oncol. *14*, 85. https://doi.org/10.1186/s13045-021-01096-0.

7. Sen, S., Won, M., Levine, M.S., Noh, Y., Sedgwick, A.C., Kim, J.S., Sessler, J.L., and Arambula, J.F. (2022). Metal-based anticancer agents as immunogenic cell death inducers: the past, present, and future. Chem. Soc. Rev. *51*, 1212–1233. https://doi.org/10.1039/D1CS00417D.

8. Malik, D., Mahendiratta, S., Kaur, H., and Medhi, B. (2021). Futuristic approach to cancer treatment. Gene *805*, 145906. https://doi.org/10.1016/j.gene.2021.145906.

9. DeVita, V.T., Jr., and Chu, E. (2008). A History of Cancer Chemotherapy. Cancer Res. *68*, 8643–8653. https://doi.org/10.1158/0008-5472.CAN-07-6611.

10. Yan, V.C., Butterfield, H.E., Poral, A.H., Yan, M.J., Yang, K.L., Pham, C.-D., and Muller, F.L. (2020). Why Great Mitotic Inhibitors Make Poor Cancer Drugs. Trends Cancer *6*, 924–941. https://doi.org/10.1016/j.trecan.2020.05.010.

11. Hani, U.,M.,Y.B., Wahab, S., Siddiqua, A., Osmani, R.A.M., and Rahamathulla, M. (2021). A Comprehensive Review of Current Perspectives on Novel Drug Delivery Systems and Approaches for Lung Cancer Management. J. Pharm. Innov. *17*, 1530–1553. https://doi.org/10.1007/s12247-021-09582-1.

12. Yu, X.-H., Hong, X.-Q., Mao, Q.-C., and Chen, W.-H. (2019). Biological effects and activity optimization of small-molecule, drug-like synthetic anion transporters. Eur. J. Med. Chem. *184*, 111782. https://doi.org/10.1016/j.ejmech.2019.111782.

13. Rezayatmand, H., Razmkhah, M., and Razeghian-Jahromi, I. (2022). Drug resistance in cancer therapy: the Pandora's Box of cancer stem cells. Stem Cell Res. Ther. *13*, 181. https://doi.org/10.1186/s13287-022-02856-6.

14. Li, G.-H., Qu, Q., Qi, T.-T., Teng, X.-Q., Zhu, H.-H., Wang, J.-J., Lu, Q., and Qu, J. (2021). Super-enhancers: a new frontier for epigenetic modifiers in cancer chemoresistance. J. Exp. Clin. Cancer Res. *40*, 174. https://doi.org/10.1186/s13046-021-01974-y.

15. Simpson, P.V., Desai, N.M., Casari, I., Massi, M., and Falasca, M. (2019). Metal-based antitumor compounds: beyond cisplatin. Future Med. Chem. *11*, 119–135. https://doi.org/10.4155/fmc-2018-0248.

16. Igney, F.H., and Krammer, P.H. (2002). Death and anti-death: tumour resistance to apoptosis. Nat. Rev. Cancer *2*, 277–288. https://doi.org/10.1038/nrc776.

17. Busschaert, N., Park, S.-H., Baek, K.-H., Choi, Y.P., Park, J., Howe, E.N.W., Hiscock, J.R., Karagiannidis, L.E., Marques, I., Félix, V., et al. (2017). A synthetic ion transporter that disrupts autophagy and induces apoptosis by perturbing cellular chloride concentrations. Nat. Chem. *9*, 667–675. https://doi.org/10.1038/nchem.2706.

18. Gale, P.A., Pérez-Tomás, R., and Quesada, R. (2013). Anion Transporters and Biological Systems. Acc. Chem. Res. *46*, 2801–2813. https://doi.org/10.1021/ar400019p.

19. Alfonso, I., and Quesada, R. (2013). Biological activity of synthetic ionophores: Ion transporters as prospective drugs? Chem. Sci. *4*, 3009–3019. https://doi.org/10.1039/c3sc50882j.

20. Roy, A., and Talukdar, P. (2021). Recent Advances in Bioactive Artificial Ionophores. Chembiochem *22*, 2925–2940. https://doi.org/10.1002/cbic.202100112.

21. Xue, J., Moyer, A., Peng, B., Wu, J., Hannafon, B.N., and Ding, W.-Q. (2014). Chloroquine Is a Zinc Ionophore. PLoS One *9*, e109180. https://doi.org/10.1371/journal.pone.0109180.

22. Kaushik, V., Yakisich, J.S., Kumar, A., Azad, N., and Iyer, A.K.V. (2018). Ionophores: Potential Use as Anticancer Drugs and Chemosensitizers. Cancers *10*, 360. https://doi.org/10.3390/cancers10100360.

23. Picci, G., Marchesan, S., and Caltagirone, C. (2022). Ion Channels and Transporters as Therapeutic Agents: From Biomolecules to Supramolecular Medicinal Chemistry. Biomedicines *10*, 885. https://doi.org/10.3390/biomedicines10040885.

24. Gale, P.A., Davis, J.T., and Quesada, R. (2017). Anion transport and supramolecular medicinal chemistry. Chem. Soc. Rev. *46*, 2497–2519. https://doi.org/10.1039/C7CS00159B.

25. Gale, P.A., Howe, E., and Wu, X. (2016). Anion Receptor Chemistry. Chem *1*, 351–422. https://doi.org/10.1016/j.chempr.2016.08.004.

26. Quesada, R. (2019). New Anionophores and Insights into Ion-Transport-Induced Cancer Cell Death. Chem *5*, 1924–1926. https://doi.org/10.1016/j.chempr.2019.07.010.

27. Park, S.-H., Park, S.-H., Howe, E.N.W., Hyun, J.Y., Chen, L.-J., Hwang, I., Vargas-Zuñiga, G., Busschaert, N., Gale, P.A., Sessler, J.L., and Shin, I. (2019). Determinants of Ion-Transporter Cancer Cell Death. Chem *5*, 2079–2098. https://doi.org/10.1016/j.chempr.2019.05.001.

28. Ko, S.-K., Kim, S.K., Share, A., Lynch, V.M., Park, J., Namkung, W., Van Rossom, W., Busschaert, N., Gale, P.A., Sessler, J.L., and Shin, I. (2014). Synthetic ion transporters can induce apoptosis by facilitating chloride anion transport into cells. Nat. Chem. *6*, 885–892. https://doi.org/10.1038/nchem.2021.

29. Casey, J.R., Grinstein, S., and Orlowski, J. (2010). Sensors and regulators of intracellular pH. Nat. Rev. Mol. Cell Biol. *11*, 50–61. https://doi.org/10.1038/nrm2820.

30. Webb, B.A., Chimenti, M., Jacobson, M.P., and Barber, D.L. (2011). Dysregulated pH: a perfect storm for cancer progression. Nat. Rev. Cancer *11*, 671–677. https://doi.org/10.1038/nrc3110.

31. Persi, E., Duran-Frigola, M., Damaghi, M., Roush, W.R., Aloy, P., Cleveland, J.L., Gillies, R.J., and Ruppin, E. (2018). Systems analysis of intracellular pH vulnerabilities for cancer therapy. Nat. Commun. *9*, 2997. https://doi.org/10.1038/s41467-018-05261-x.

32. Bailey, K.M., Wojtkowiak, J.W., Hashim, A.I., and Gillies, R.J. (2012). Chapter Four - Targeting the Metabolic Microenvironment of Tumors. In Current Challenges in Personalized Cancer Medicine, K. S. M. B. T.-A., P. Smalley, ed. (Academic Press), pp. 63–107. https://doi.org/10.1016/B978-0-12-397927-8.00004-X.

33. Wu, X., Howe, E.N.W., and Gale, P.A. (2018). Supramolecular Transmembrane Anion Transport: New Assays and Insights. Acc. Chem. Res. *51*, 1870–1879. https://doi.org/10.1021/acs.accounts.8b00264.

34. Danby, P.M., Lombardi, C., Meanwell, M., and Fyles, T. (2017). Electrogenic transport by lipophilic guanidinium salts as anion carriers in bilayer membranes. Supramol. Chem. *29*, 585–599. https://doi.org/10.1080/10610278.2017.1299865.

35. Wu, X., and Gale, P.A. (2021). Measuring anion transport selectivity: a cautionary tale. Chem. Commun. *57*, 3979–3982. https://doi.org/10.1039/D1CC01038G.

36. Motloch, P., Guerreiro, A., Azeredo, C.Q., Bernardes, G.J.L., Hunter, C.A., and Kocsis, I. (2019). Triaminopyrimidine derivatives as transmembrane HCl transporters. Org. Biomol. Chem. *17*, 5633–5638. https://doi.org/10.1039/C9OB00725C.

37. Chen, L.-J., Wu, X., Gilchrist, A.M., and Gale, P.A. (2022). Organoplatinum Compounds as Anion-Tuneable Uphill Hydroxide Transporters. Angew Chem. Int. Ed. Engl. *61*, e202116355. https://doi.org/10.1002/anie.202116355.

38. Chattopadhayay, S., Ghosh, A., Kumar Mukhopadhyay, T., Sharma, R., Datta, A., and Talukdar, P. (2023). Supramolecular Barrel-Rosette Ion Channel Based on 3,5-Diaminobenzoic Acid for Cation-Anion Symport. Angew Chem. Int. Ed. Engl. *62*, e202313712. https://doi.org/10.1002/anie.202313712.

39. Mondal, A., Malla, J.A., Paithankar, H., Sharma, S., Chugh, J., and Talukdar, P. (2021). A Pyridyl-Linked Benzimidazolyl Tautomer Facilitates Prodigious H+/Cl– Symport through a Cooperative Protonation and Chloride Ion Recognition. Org. Lett. *23*, 6131–6136. https://doi.org/10.1021/acs.orglett.1c02235.

40. Alonso-Carrillo, D., Arias-Betancur, A., Carreira-Barral, I., Fontova, P., Soto-Cerrato, V., García-Valverde, M., Pérez-Tomás, R., and Quesada, R. (2023). Small molecule anion carriers facilitate lactate transport in model liposomes and cells. iScience *26*, 107898. https://doi.org/10.1016/j.isci.2023.107898.

41. de Jong, J., Bos, J.E., and Wezenberg, S.J. (2023). Stimulus-Controlled Anion Binding and Transport by Synthetic Receptors. Chem. Rev. *123*, 8530–8574. https://doi.org/10.1021/acs.chemrev.3c00039.

42. Akhtar, N., Biswas, O., and Manna, D. (2020). Biological applications of synthetic anion transporters. Chem. Commun. *56*, 14137–14153. https://doi.org/10.1039/D0CC05489E.

43. Tosolini, M., Pengo, P., and Tecilla, P. (2018). Biological Activity of Trans-Membrane Anion Carriers. Curr. Med. Chem. *25*, 3560–3576. https://doi.org/10.2174/0929867325666180309113222.

44. Valls, A., Altava, B., Aseyev, V., Carreira-Barral, I., Conesa, L., Falomir, E., García-Verdugo, E., Luis, S.V., and Quesada, R. (2021). Structure–antitumor activity relationships of tripodal imidazolium-amino acid based salts. Effect of the nature of the amino acid, amide substitution and anion. Org. Biomol. Chem. *19*, 10575–10586. https://doi.org/10.1039/D1OB01825F.

45. Jowett, L.A., Howe, E.N.W., Soto-Cerrato, V., Van Rossom, W., Pérez-Tomás, R., and Gale, P.A. (2017). Indole-based perenosins as highly potent HCl transporters and potential anti-cancer agents. Sci. Rep. *7*, 9397. https://doi.org/10.1038/s41598-017-09645-9.

46. Busschaert, N., and Gale, P.A. (2013). Small-Molecule Lipid-Bilayer Anion Transporters for Biological Applications. Angew Chem. Int. Ed. Engl. *52*, 1374–1382. https://doi.org/10.1002/anie.201207535.

47. Kumar, N., and Madhavan, N. (2023). Small molecule-derived pH-gated ion transporters. Org. Biomol. Chem. *21*, 5892–5905. https://doi.org/10.1039/D3OB00496A.

48. Howe, E.N.W., Busschaert, N., Wu, X., Berry, S.N., Ho, J., Light, M.E., Czech, D.D., Klein, H.A., Kitchen, J.A., and Gale, P.A. (2016). pH-Regulated Nonelectrogenic Anion Transport by Phenylthiosemicarbazones. J. Am. Chem. Soc. *138*, 8301–8308. https://doi.org/10.1021/jacs.6b04656.

49. Santacroce, P.V., Davis, J.T., Light, M.E., Gale, P.A., Iglesias-Sánchez, J.C., Prados, P., and Quesada, R. (2007). Conformational Control of Transmembrane Cl^- Transport. J. Am. Chem. Soc. *129*, 1886–1887. https://doi.org/10.1021/ja068067v.

50. Busschaert, N., Elmes, R.B.P., Czech, D.D., Wu, X., Kirby, I.L., Peck, E.M., Hendzel, K.D., Shaw, S.K., Chan, B., Smith, B.D., et al. (2014). Thiosquaramides: pH switchable anion transporters. Chem. Sci. *5*, 3617–3626. https://doi.org/10.1039/C4SC01629G.

51. Elmes, R.B.P., Busschaert, N., Czech, D.D., Gale, P.A., and Jolliffe, K.A. (2015). pH switchable anion transport by an oxothiosquaramide. Chem. Commun. *51*, 10107–10110. https://doi.org/10.1039/C5CC03625A.

52. Rastogi, S., Marchal, E., Uddin, I., Groves, B., Colpitts, J., McFarland, S.A., Davis, J.T., and Thompson, A. (2013). Synthetic prodigiosenes and the influence of C-ring substitution on DNA cleavage, transmembrane chloride transport and basicity. Org. Biomol. Chem. *11*, 3834–3845. https://doi.org/10.1039/C3OB40477C.

53. Howe, E.N.W., Chang, V.-V.T., Wu, X., Fares, M., Lewis, W., Macreadie, L.K., and Gale, P.A. (2022). Halide-selective, proton-coupled anion transport by phenylthiosemicarbazones. Biochim. Biophys. Acta Biomembr. *1864*, 183828. https://doi.org/10.1016/j.bbamem.2021.183828.

54. Roy, A., Saha, D., Mandal, P.S., Mukherjee, A., and Talukdar, P. (2017). pH-Gated Chloride Transport by a Triazine-Based Tripodal Semicage. Chem. Eur J. *23*, 1241–1247. https://doi.org/10.1002/chem.201605033.

55. Wang, Z.-K., Hong, X.-Q., Hu, J., Xing, Y.-Y., and Chen, W.-H. (2021). Synthesis and biological activity of squaramido-tethered bisbenzimidazoles as synthetic anion transporters. RSC Adv. *11*, 3972–3980. https://doi.org/10.1039/D0RA10189C.

56. Marchetti, L.A., Krämer, T., and Elmes, R.B.P. (2022). Amidosquaramides – a new anion binding motif with pH sensitive anion transport properties. Org. Biomol. Chem. *20*, 7056–7066. https://doi.org/10.1039/D2OB01176J.

57. Gerweck, L.E., Vijayappa, S., and Kozin, S. (2006). Tumor pH controls the in vivo efficacy of weak acid and base chemotherapeutics. Mol. Cancer Therapeut. *5*, 1275–1279. https://doi.org/10.1158/1535-7163.MCT-06-0024.

58. Wu, X., Small, J.R., Cataldo, A., Withecombe, A.M., Turner, P., and Gale, P.A. (2019). Voltage-Switchable HCl Transport Enabled by Lipid Headgroup–Transporter Interactions. Angew Chem. Int. Ed. Engl. *58*, 15142–15147. https://doi.org/10.1002/anie.201907466.

59. Martínez-Crespo, L., Hewitt, S.H., De Simone, N.A., Šindelář, V., Davis, A.P., Butler, S., and Valkenier, H. (2021). Transmembrane Transport of Bicarbonate Unravelled. Chem. Eur J. *27*, 7367–7375. https://doi.org/10.1002/chem.202100491.

60. Cheung, S., Wu, D., Daly, H.C., Busschaert, N., Morgunova, M., Simpson, J.C., Scholz, D., Gale, P.A., and O'Shea, D.F. (2018). Real-Time Recording of the Cellular Effects of the Anion Transporter Prodigiosin. Chem *4*, 879–895. https://doi.org/10.1016/j.chempr.2018.02.009.

61. Tapia, L., Alfonso, I., and Solà, J. (2021). Molecular cages for biological applications. Org. Biomol. Chem. *19*, 9527–9540. https://doi.org/10.1039/D1OB01737C.

62. Martí, I., Bolte, M., Burguete, M.I., Vicent, C., Alfonso, I., and Luis, S.V. (2014). Tight and selective caging of chloride ions by a pseudopeptidic host. Chem. Eur J. *20*,

7458–7464. https://doi.org/10.1002/chem.201303604.

63. Martí, I., Rubio, J., Bolte, M., Burguete, M.I., Vicent, C., Quesada, R., Alfonso, I., and Luis, S.V. (2012). Tuning chloride binding, encapsulation, and transport by peripheral substitution of pseudopeptidic tripodal small cages. Chem. Eur J. *18*, 16728–16741. https://doi.org/10.1002/chem.201202182.

64. Tapia, L., Pérez, Y., Bolte, M., Casas, J., Solà, J., Quesada, R., and Alfonso, I. (2019). pH-Dependent Chloride Transport by Pseudopeptidic Cages for the Selective Killing of Cancer Cells in Acidic Microenvironments. Angew Chem. Int. Ed. Engl. *58*, 12465–12468. https://doi.org/10.1002/anie.201905965.

65. Gillis, E.P., Eastman, K.J., Hill, M.D., Donnelly, D.J., and Meanwell, N.A. (2015). Applications of Fluorine in Medicinal Chemistry. J. Med. Chem. *58*, 8315–8359. https://doi.org/10.1021/acs.jmedchem.5b00258.

66. Valkenier, H., Akrawi, O., Jurček, P., Sleziaková, K., Lízal, T., Bartik, K., and Šindelář, V. (2019). Fluorinated Bambusurils as Highly Effective and Selective Transmembrane $Cl^{-}/HCO3^{-}$ Antiporters. Chem *5*, 429–444. https://doi.org/10.1016/j.chempr.2018.11.008.

67. Ojima, I. (2013). Exploration of Fluorine Chemistry at the Multidisciplinary Interface of Chemistry and Biology. J. Org. Chem. *78*, 6358–6383. https://doi.org/10.1021/jo400301u.

68. Shinada, N.K., de Brevern, A.G., and Schmidtke, P. (2019). Halogens in Protein–Ligand Binding Mechanism: A Structural Perspective. J. Med. Chem. *62*, 9341–9356. https://doi.org/10.1021/acs.jmedchem.8b01453.

69. Coenen, H.H., and Ermert, J. (2018). ^{18}F-labelling innovations and their potential for clinical application. Clin. Transl. Imaging *6*, 169–193. https://doi.org/10.1007/s40336-018-0280-0.

70. Deng, X., Rong, J., Wang, L., Vasdev, N., Zhang, L., Josephson, L., and Liang, S.H. (2019). Chemistry for Positron Emission Tomography: Recent Advances in ^{11}C-^{18}F-^{13}N-and ^{15}O-Labeling Reactions. Angew Chem. Int. Ed. Engl. *58*, 2580–2605. https://doi.org/10.1002/anie.201805501.

71. Filler, R., and Saha, R. (2009). Fluorine in medicinal chemistry: a century of progress and a 60-year retrospective of selected highlights. Future Med. Chem. *1*, 777–791. https://doi.org/10.4155/fmc.09.65.

72. Hagmann, W.K. (2008). The Many Roles for Fluorine in Medicinal Chemistry. J. Med. Chem. *51*, 4359–4369. https://doi.org/10.1021/jm800219f.

73. Vacca, A., Francesconi, O., and Roelens, S. (2012). BC_{50}: A Generalized, Unifying Affinity Descriptor. Chem. Rec. *12*, 544–566. https://doi.org/10.1002/tcr.201200014.

74. Razgulin, A.V., and Mecozzi, S. (2006). Binding Properties of Aromatic Carbon-Bound Fluorine. J. Med. Chem. *49*, 7902–7906. https://doi.org/10.1021/jm0600702.

75. Gilchrist, A.M., Wang, P., Carreira-Barral, I., Alonso-Carrillo, D., Wu, X., Quesada, R., and Gale, P.A. (2021). Supramolecular methods: the 8-hydroxypyrene-1,3,6-trisulfonic acid (HPTS) transport assay. Supramol. Chem. *33*, 325–344. https://doi.org/10.1080/10610278.2021.1999956.

76. Marques, I., Costa, P.M.R., Q Miranda, M., Busschaert, N., Howe, E.N.W., Clarke, H.J., Haynes, C.J.E., Kirby, I.L., Rodilla, A.M., Pérez-Tomás, R., et al. (2018). Full elucidation of the transmembrane anion transport mechanism of squaramides using in silico investigations. Phys. Chem. Chem. Phys. *20*, 20796–20811. https://doi.org/10.1039/c8cp02576b.

77. Roux, B. (1995). The calculation of the potential of mean force using computer simulations. Comput. Phys. Commun. *91*, 275–282. https://doi.org/10.1016/0010-4655(95)00053-I.